J. Fluid Mech. (1990), *vol.* 214, *pp.* 89–110
Printed in Great Britain

Higher-order boundary-layer solution for unsteady motion of a circular cylinder

By SOONIL NAM
Department of Mechanical Engineering, Stanford University, Stanford, CA 94305, USA

(Received 6 May 1988 and in revised form 6 October 1989)

The higher-order boundary-layer solution for an impulsively started circular cylinder with uniform velocity and for an exponentially accelerating cylinder in incompressible, relatively high-Reynolds-number flow of short duration are considered. A perturbation method is employed to linearize the two-dimensional vorticity transport equation by a double series expansion with respect to the Reynolds number and the time. A matched asymptotic expansion is carried out to define the proper boundary conditions between the viscous and inviscid layers for the linearized first-, second-, and third-order boundary-layer equations. Singularities appear in the higher-order approximate solutions to the viscous displacement velocities and skin frictions, which coincide with the singularity of the first-order approximate solution. These singularities have alternating signs and increasing magnitudes, thus attempting to remove the effects of the singularity of the lower-order solution. However, this futile attempt at removing a singularity by superposing even stronger singularities makes the solution worse around the singularity, which shows that the singularity is an artifact of the thin-boundary-layer approximation.

1. Introduction

Recently there have been many arguments on the existence and nature of a singularity in unsteady boundary-layer flow analogous to the Goldstein (1948) singularity in steady boundary-layer flow.

After Blasius (1908) initially investigated the flow past an impulsively started circular cylinder as a function of time with a boundary-layer approximation, Goldstein & Rosenhead (1936), Wang (1967), Collins & Dennis (1973*a*, *b*), Telionis & Tsahalis (1974), Bar-Lev & Yang (1975), Cebeci (1979), Wang (1979), van Dommelen & Shen (1980), Cowley (1983), Ingham (1984), and recently Henkes & Veldman (1987) have followed. Sears & Telionis (1971), van Dommelen & Shen (1980), Ingham (1984), and Henkes & Veldman (1987) have suggested some connection between the singularity and separation. After van Dommelen & Shen (1980) clearly showed that a singularity exists at $\tau \approx 1.5$, where τ is a dimensionless time normalized by a/U_∞, i.e. radius/velocity of the cylinder, it seems that the controversy over the existence of a singularity in the boundary-layer solution of unsteady flow had been put to rest. Cowley (1983) and Ingham (1984) both confirmed this result

All the previous work done thus far regarding this unsteady flow singularity has been concerned only with the first-order boundary-layer approximation (or classical boundary-layer approximation). No information on the singularity of higher-order approximations is available yet.

The higher-order approximation is closer to the full Navier–Stokes equations than

the first-order approximation. Hence if our expansion is physically sound, it should ease the singularity which we experience in the first-order solution. Otherwise it will reveal a similar behaviour to the thin-airfoil expansion for the potential flow past an ellipse (Van Dyke 1975, p. 51). In this example the thin-airfoil assumption has been violated around the stagnation point. In response, the first-order solution yields a singularity at the stagnation point, then each following higher-order solution tries to compensate for the singularity caused by the previous approximation with a larger magnitude and an alternating sign; in consequence the singularity is compounded in the higher approximation. If this happens in our higher-order solutions, we can identify that we have violated some physical grounds in our approximation.

For this purpose, two models are used in this work: the flow past an impulsively started circular cylinder and the flow past an exponentially accelerating circular cylinder. The latter problem has been treated by Watson (1955) who obtained a three-term solution with respect to time for the classical boundary-layer approximation. Contrary to the impulsively started cylinder, which possesses an initial inherent singularity by its sudden movement, the exponentially moving cylinder does not have an discontinuity. It starts from rest very slowly at $\tau \to -\infty$ and moves smoothly with a speed that increases exponentially with time. Therefore comparing the results of these two models will determine whether the singularity arises from the impulsive movement.

For both cases, the approximation has been extended to third order with respect to Reynolds number Re, where $Re = U_\infty a/\nu$, and a perturbation method has been employed to linearize the two-dimensional vorticity equation by a double series expansion with respect to Re and time.

2. Impulsively started circular cylinder

We consider the motion of a viscous, incompressible fluid around a circular cylinder of infinite length which suddenly starts to move with constant velocity perpendicular to its axis as shown in figure 1.

The governing equation is the two-dimensional vorticity transport equation for the incompressible flow:

$$\begin{aligned}
&\Psi_{rrt}+\frac{1}{r}\psi_{rt}+\frac{1}{r^2}\Psi_{\theta\theta t}+\frac{1}{r}\Psi_r\Psi_{\theta rr}+\frac{1}{r^2}\Psi_{r\theta}\Psi_r+\frac{1}{r^3}\Psi_{\theta\theta\theta}\Psi_r \\
&\qquad -\frac{1}{r}\Psi_{rrr}\Psi_\theta+\frac{1}{r^3}(\Psi_r\Psi_\theta-\Psi_{\theta\theta r}\Psi_\theta)-\frac{1}{r^2}\Psi_{rr}\Psi_\theta+\frac{2}{r^4}\Psi_{\theta\theta}\Psi_\theta \\
&= \nu\left(\Psi_{rrrr}+\frac{1}{r^4}\Psi_{\theta\theta\theta\theta}+\frac{2}{r}\Psi_{rrr}+\frac{2}{r^2}\Psi_{rr\theta\theta}-\frac{2}{r^3}\Psi_{\theta\theta r}-\frac{1}{r^2}\Psi_{rr}+\frac{4}{r^4}\Psi_{\theta\theta}+\frac{1}{r^3}\Psi_r\right), \quad (2.1)
\end{aligned}$$

where Ψ is the stream function, $u = \Psi_r$, and $v = -(1/r)\Psi_\theta$, with boundary conditions

$$\Psi = \Psi_r = 0 \quad \text{at} \quad r = a, \tag{2.2a}$$

$$\Psi = 0 \quad \text{at} \quad t = 0, \tag{2.2b}$$

$$\Psi_r \to U_\infty \sin\theta \quad \text{as} \quad r \to \infty, \quad t > 0. \tag{2.2c}$$

After transforming coordinates into the usual boundary-layer coordinates in which y is normal to the surface and x is measured along the surface from the front

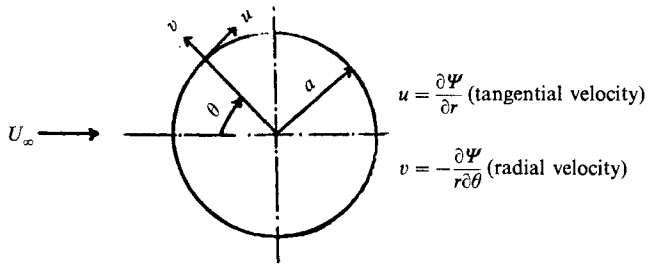

FIGURE 1. Flow past a circular cylinder.

stagnation point, and collecting terms which have the same order of magnitude, the governing equation (2.1) may be arranged as follows:

$$\begin{aligned}\Psi_{yyt}-\nu\Psi_{yyyy} = &\left\{[-\Psi_y\Psi_{xyy}+\Psi_x\Psi_{yyy}]\right.\\ &\left.-\frac{1}{a}\Psi_{yt}+\frac{2\nu}{a}\Psi_{yyy}-\frac{1}{a}\Psi_{xy}\Psi_y+\frac{1}{a}\Psi_{yy}\Psi_x+\frac{y}{a}\Psi_y\Psi_{xyy}-\frac{y}{a}\Psi_{yyy}\Psi_x\right\}\\ &-\Psi_{xxt}+2\nu\Psi_{yyxx}-\frac{\nu}{a^2}\Psi_{yy}-\Psi_{xxx}\Psi_y-\frac{\Psi_y\Psi_x}{a^2}+\Psi_{xxy}\Psi_x+\frac{y}{a^2}\Psi_{yt}\\ &+\frac{2y}{a^2}\Psi_{xy}\Psi_y-\frac{\nu^2 y}{a^2}\Psi_{yyy}-\frac{2y}{a^2}\Psi_{yy}\Psi_x-\frac{y^2}{a^2}\Psi_y\Psi_{xyy}+\frac{y^2}{a^2}\Psi_x\Psi_{yyy}\\ &+O(\delta^2). \qquad (2.3)\end{aligned}$$

In the boundary layer, we regard y and Ψ as of $O(\delta)$, ν of $O(\delta^2)$, and x and t as of $O(1)$, where δ is a boundary-layer thickness non-dimensionalized by a. The terms in square brackets in (2.3) are only of $O(1/\delta)$, the terms in curly brackets are of $O(1)$, and the complete equation (2.3) contains $O(\delta)$ terms; consequently we call these first-order, second-order, and third-order approximations, respectively. Here approximations only up to third-order have been considered.

2.1. *First-order (classical) boundary-layer expansion*

In addition to $\Psi(x,0,t) = \Psi_y(x,0,t) = 0$, two more boundary conditions should be supplied by the inner–outer-layer matching to solve the first-order approximation to (2.3) (i.e. that in square brackets).

The basic inviscid approximation gives the first-order potential-flow solution

$$\bar{\Psi} = U_\infty\left(r-\frac{a^2}{r}\right)\sin\theta, \qquad (2.4)$$

where $\bar{\Psi}$ represents a stream function for the potential flow. We introduce the stretched coordinate variable $\eta = y/2(\nu t)^{\frac{1}{2}}$, and the dimensionless time $\tau = U_\infty t/a$. Then (2.4) shows that Ψ may be expanded as

$$\Psi = 4(\nu t)^{\frac{1}{2}}U_\infty\left[\tilde{\psi}(\eta,\theta,\tau)+\frac{(\nu t)^{\frac{1}{2}}}{a}\tilde{\tilde{\psi}}(\eta,\theta,\tau)+\frac{\nu t}{a^2}\tilde{\tilde{\tilde{\psi}}}(\eta,\theta,\tau)+O\left(\frac{(\nu t)^{\frac{3}{2}}}{a^3}\right)\right], \qquad (2.5)$$

where $\tilde{\psi}, \tilde{\tilde{\psi}}, \tilde{\tilde{\tilde{\psi}}}$ refer to the dimensionless stream function of the first-, second-, and third-order approximate solution, respectively. Here we have used an expansion parameter $(\nu t)^{\frac{1}{2}}/a$. The solution is expanded first with respect to $(\nu t)^{\frac{1}{2}}/a$ according to

each order of approximation, then each non-dimensional stream function is expanded with respect to dimensionless time. Here $(\nu t)^{\frac{1}{2}}/a$ is equivalent to $(\tau/Re)^{\frac{1}{2}}$, where Re/τ is the so-called *unsteady Reynolds number*. Since the boundary-layer thickness depends strongly on both Re and the elapsed time after the impulsive start of the body, the choice of these two expansion parameters seems quite proper.

After following inner–outer matching procedures which are given by Van Dyke (1975, p. 90), we get

$$\bar{\Psi} = 4(\nu t)^{\frac{1}{2}} U_\infty \left[\eta \sin\theta + O\left(\frac{(\nu t)^{\frac{1}{2}}}{a}\right)\right]. \tag{2.6}$$

From this first-order matching between (2.6) and (2.5) we get $\Psi \sim 4(\nu t)^{\frac{1}{2}} U_\infty \eta \sin\theta$ as $\eta \to \infty$, which gives the boundary condition $\Psi_y \to 2U_\infty \sin\theta$ as $y \to \infty$. The integration of the first-order approximation to (2.3) with respect to y combined with this matching condition and the zero velocity on the wall condition yields a simpler version of the first-order boundary-layer equation:

$$\Psi_{yt} - \nu \Psi_{yyy} = -\Psi_y \Psi_{xy} + \Psi_x \Psi_{yy} + \frac{4U_\infty^2}{a} \sin\theta \cos\theta. \tag{2.7}$$

The non-dimensionalization of (2.7) by using dimensionless stretched coordinates combined with (2.5) results in

$$\tilde{\psi}_{\eta\eta\eta} + 2\eta \tilde{\psi}_{\eta\eta} - 4\tau \tilde{\psi}_{\eta\tau} = 8\tau(\tilde{\psi}_\eta \tilde{\psi}_{\eta\theta} - \tilde{\psi}_\theta \tilde{\psi}_{\eta\eta} - \sin\theta\cos\theta). \tag{2.8}$$

We expand the dimensionless stream function with respect to dimensionless time as

$$\tilde{\psi} = \sum_{p=0}^{\infty} \tau^p \phi_p(\eta, \theta). \tag{2.9}$$

We again expand ϕ_p as

$$\phi_p = \sum_{q=1}^{p+1} f_{pq}(\eta) \sin q\theta, \tag{2.10}$$

since Ψ must satisfy the pressure term which is expressed in the last term in (2.7), and we also assume that the flow is symmetrical about the direction of motion of the cylinder until the solution breaks down. By substituting (2.9), (2.10) into (2.8), we can transform the partial differential equation to the corresponding ordinary differential equations. After rearranging the nonlinear terms and equating the coefficients of each of the $\sin q\theta$ terms, (following Cowley 1983), it is found that if $p+q$ is even then $f_{pq} = 0$, and that if $p+q$ is odd then

$$f'''_{pq} + 2\eta f''_{pq} - 4p f'_{pq} = 4(S_{1pq} + S_{2pq} - S_{3pq} - \delta_{1p}). \tag{2.11}$$

The double sums S_{ipq} are given by

$$S_{1pq} = \sum_{j=0}^{p-1} \sum_{n=\max(1,\,q+j-p)}^{\min(j+1,\,q-1)} n(f'_{jn} f'_{kq-n} - f_{jn} f''_{kq-n}), \tag{2.12a}$$

$$S_{2pq} = \sum_{j=0}^{p-1-q} \sum_{n=1}^{\min(j+1,\,p-j-q)} n(f'_{jn} f'_{kq+n} - f_{jn} f''_{kq+n}), \tag{2.12b}$$

$$S_{3pq} = \sum_{j=q}^{p-1} \sum_{n=q+1}^{\min(j+1,\,p-j+q)} n(f'_{jn} f'_{kn-q} - f_{jn} f''_{kn-q}), \tag{2.12c}$$

where $k = p-1-j$, and the sums are zero if the upper index is less than the lower one.

The prime denotes differentiation with respect to η throughout present work. Also the boundary conditions (2.2*a*, *b*, *c*) give

$$f_{pq}(0) = f'_{pq}(0) = 0 \quad \text{for all } p \text{ and } q, \tag{2.13a}$$

$$f'_{01} \to 1, \quad f'_{pq} \to 0 \quad \text{for all other } p \text{ and } q \quad \text{as } \eta \to \infty. \tag{2.13b}$$

The analytic solution of the first term is

$$f_{01} = \eta \operatorname{erf} \eta + \frac{1}{\pi^{\frac{1}{2}}}(e^{-\eta^2} - 1), \tag{2.14}$$

which is same as the solution of the Stokes' first problem for a flat plate set impulsively into motion.

The quickly growing right-hand side of (2.11) forced us to use numerical means. We decided to adopt a finite-difference method to solve these equations. We limit our expansion to 51 dimensionless time terms, mainly because of the huge memory size requirement when we use a finite-difference method. This appears to be the minimum number of terms to deduce any worthwhile results according to Cowley (1983). Then the number of equations of the form of (2.11) which we have to solve for the first expansion is 676. Since we intended to go on to the third approximation, the total number of equations we need to solve by numerical means is 2028.

Following Collins & Dennis (1973*a*), we developed an $O(h^4)$-accuracy finite-difference method, where h is mesh size. By substituting $F_{pq} = e^{\frac{1}{2}\eta^2} f'_{pq}$, the general form of (2.11) becomes

$$F''_{pq} - (4p + 1 + \eta^2) F_{pq} = 4 e^{\frac{1}{2}\eta^2} (S_{1pq} + S_{2pq} - S_{3pq} - \delta_{1p}). \tag{2.15}$$

Details of how to solve this equation with $O(h^4)$ accuracy are given by Fox (1957), Collins & Dennis (1973*a*) and Cowley (1983). Though Fox's method guarantees accuracy of $O(h^4)$, we modified the program slightly using the technique of Richardson's extrapolation to improve the accuracy of the program to $O(h^6)$. After obtaining numerical solutions of F_{pq}, we derived the stream function and vorticity function by numerical integration and numerical differentiation, respectively.

A very fine mesh was required to get high precision in higher-order time terms in order to locate the singular point. We found that using $h = 0.0125$ gives an optimum trade-off size between truncation error and round-off error if we use an $O(h^6)$ method and double precision. Smaller mesh sizes actually yield more rapidly growing errors due to a round-off effect in our scheme. The problem contains a boundary condition at $\eta \to \infty$, and we have chosen $\eta = 10$ as suitably large to enforce this condition in our numerical scheme.

The computation was done on a Convex C-1 machine with vectorization option. The accuracy appeared to be deteriorating as the number of computations increases, however through the whole process the accuracy remained at an acceptable level.

2.2. *Second-order boundary-layer expansion*

After we obtain the non-dimensionalized second-order boundary-layer equation by inserting (2.5) into the second-order approximation to (2.3), i.e. the terms in curly brackets, we expand the second-order dimensionless stream function as

$$\tilde{\psi} = \sum_{p=0}^{\infty} \sum_{q=1}^{p+1} \tau^p g_{pq}(\eta) \sin q\theta. \tag{2.16}$$

This gives the ODE's for the second-order boundary-layer problem for $p+q$ odd as

$$g''''_{pq}+2\eta g'''_{pq}-4pg''_{pq}=4(-\eta f''_{pq}-f'''_{pq}+2pf'_{pq})+4(S_{1pq}+S_{2pq}-S_{3pq}). \tag{2.17}$$

The double sums S_{ipq} are given by

$$S_{1pq}=\sum_{j=0}^{p-1}\sum_{n=\max(1,\,q+j-p)}^{\min(j+1,\,q-1)} n[f'''_{jn}g'_{kq-n}+g''_{jn}f'_{kq-n}-f_{jn}g'''_{kq-n}$$
$$-g_{jn}f'''_{kq-n}+2(f'_{jn}f'_{kq-n}-f_{jn}f''_{kq-n})+2\eta(f_{jn}f'''_{kq-n}-f''_{jn}f'_{kq-n})], \tag{2.18a}$$

$$S_{2pq}=\sum_{j=0}^{p-1-q}\sum_{n=1}^{\min(j+1,\,p-j-q)} n[f'''_{jn}g'_{kq+n}+g''_{jn}f'_{kq+n}-f_{jn}g'''_{kq+n}$$
$$-g_{jn}f'''_{kq+n}+2(f'_{jn}f'_{kq+n}-f_{jn}f''_{kq+n})+2\eta(f_{jn}f'''_{kq+n}-f''_{jn}f'_{kq+n})], \tag{2.18b}$$

$$S_{3pq}=\sum_{j=q}^{p-1}\sum_{n=q+1}^{\min(j+1,\,p-j+q)} n[f'''_{jn}g'_{kn-q}+g''_{jn}f'_{kn-q}-f_{jn}g'''_{kn-q}$$
$$-g_{jn}f'''_{kn-q}+2(f'_{jn}f'_{kn-q}-f_{jn}f''_{kn-q})+2\eta(f_{jn}f'''_{kn-q}-f''_{jn}f'_{kn-q})]. \tag{2.18c}$$

In addition to $g_{pq}(0)=0$ and $g'_{pq}(0)=0$, two more sets of boundary conditions are provided by the matching conditions.

The second-order outer-layer solution is determined from the first-order inner expansion. Then the second-order outer-layer solution gives the matching condition for the second-order inner solution.

Rewriting the complete solution of the first-order boundary layer in outer variables and expanding for small $(\nu t)^{\frac{1}{2}}/a$ yields

$$\bar{\Psi}=U_\infty\left\{\left[2(r-a)-\frac{4(\nu t)^{\frac{1}{2}}}{\pi^{\frac{1}{2}}}\right]\sin\theta+4(\nu t)^{\frac{1}{2}}\sum_{p=1}^{\infty}\sum_{q=2}^{p+1}\tau^p f_{pq}\sin q\theta\right\}. \tag{2.19}$$

This inner solution (2.19) determines the coefficients of the second-order potential-flow solution, which follows.

The general solution of the second-order approximate potential flow is

$$\Psi=U_\infty\left[\left(r-\frac{a^2}{r}\right)\sin\theta+\sum_{q=1}^{\infty}\frac{C_q a^q}{r^q}\sin q\theta\right]. \tag{2.20}$$

Since the inner solution (2.19) shows that the second-order expansion in outer variables has an expression in terms of $(\nu t)^{\frac{1}{2}}$ and τ, we assume the coefficient C_q to be

$$C_q=\sum_{p=0}^{\infty}\tau^p[(\nu t)^{\frac{1}{2}}\alpha_{pq}], \tag{2.21}$$

where α_{pq} is a constant, to satisfy dimensions. Rewriting the assumed solution with inner variables and expanding for small $(\nu t)^{\frac{1}{2}}/a$, comparison between the inner and outer solutions determines the coefficients C_q as

$$C_q=(\nu t)^{\frac{1}{2}}\left[-\frac{4}{\pi^{\frac{1}{2}}}\delta_{1q}+\sum_{p=1}^{\infty}4\tau^p f_{pq}(\infty)\right]. \tag{2.22}$$

Rewriting the second-order potential-flow solution in inner variables and expanding for small $(\nu t)^{\frac{1}{2}}/a$ shows that the matching conditions for the second-order boundary-layer solution are that as $\eta\to\infty$

$$g_{01}\sim-\eta^2+\frac{2}{\pi^{\frac{1}{2}}}\eta, \tag{2.23a}$$

$$g_{pq}\sim-2qf_{pq}(\infty)\eta, \quad 1\leqslant p. \tag{2.23b}$$

The analytic solution for the first term of the second-order boundary-layer equation is

$$g_{01} = (-\tfrac{3}{2}\eta^2 - \tfrac{1}{4})\operatorname{erf}\eta - \frac{3}{2\pi^{\frac{1}{2}}}\eta\, e^{-\eta^2} + \tfrac{1}{2}\eta^2 + \frac{2}{\pi^{\frac{1}{2}}}\eta, \tag{2.24}$$

which agrees with Wang (1967), Collins & Dennis (1973*a*). Bar-Lev & Yang (1975) made a typographic error in their solution.

Once again by adopting $G_{pq} = e^{\frac{1}{2}\eta^2} g''_{pq}$, we transformed (2.17) to second-order ODE's to get numerical solutions. We need to supply the value of $g''_{pq}(0)$ as one of the boundary conditions to get the numerical solution. Since it is impossible to know this value in advance, the following scheme was conceived. First, we assume two different values for $g''_{pq}(0)$ and carry out numerical computations with each of these two conditions. Then we calculate $g'_{pq}(\infty)$ by numerical integration for each of these two solutions. Next we construct a linear combination of the two solutions that gives the correct $g'_{pq}(\infty)$ obtained by the matching condition. The proper $g''_{pq}(0)$ is formed from the linear combination above.

2.3. *Third-order boundary-layer expansion*

We expand the third-order dimensionless stream function as

$$\tilde{\tilde{\psi}} = \sum_{p=0}^{\infty} \sum_{q=1}^{p+1} \tau^p h_{pq}(\eta) \sin q\theta, \tag{2.25}$$

then the ODE's for the third-order equations $p+q$ odd are

$$\begin{aligned} h'''_{pq} + 2\eta h''_{pq} - 2h'_{pq} - 4p h'_{pq} = 4[&-g'''_{pq} - \eta g''_{pq} + g'_{pq} + 2p(g'_{pq} - 2q^2 f_{pq} - 2\eta f'_{pq}) \\ &+ 2q^2(-f_{pq} + \eta f'_{pq} + f''_{pq}) + (2\eta^2+1) f''_{pq} + 2\eta f'''_{pq} + (S_{1pq} + S_{2pq} - S_{3pq})]. \end{aligned} \tag{2.26}$$

The double sums S_{ipq} are given by

$$\begin{aligned} S_{1pq} = \sum_{j=0}^{p-1} \sum_{n=\max(1,\, q+j-p)}^{\min(j+1,\, q-1)} & n\{f''_{jn} h'_{kq-n} + g''_{jn} g'_{kq-n} + h''_{jn} f'_{kq-n} - f_{jn} h'''_{kq-n} \\ & - g_{jn} g'''_{kq-n} - h_{jn} f'''_{kq-n} + 2(f'_{jn} g'_{kq-n} + g'_{jn} f'_{kq-n} - g_{jn} f''_{kq-n} - f_{jn} g''_{kq-n}) \\ & + 2\eta(-g''_{jn} f'_{kq-n} - f''_{jn} g'_{kq-n} + f_{jn} g'''_{kq-n} + g_{jn} f'''_{kq-n} + 4 f_{jn} f''_{kq-n} - 4 f'_{jn} f'_{kq-n}) \\ & + 4[(q-n)^2 - n^2 + 1](f_{jn} f'_{kq-n}) + 4\eta^2(f''_{jn} f'_{kq-n} - f_{jn} f'''_{kq-n})\}, \end{aligned} \tag{2.27a}$$

$$\begin{aligned} S_{2pq} = \sum_{j=0}^{p-1-q} \sum_{n=1}^{\min(j+1,\, p-j-q)} & n\{f''_{jn} h'_{kq+n} + g''_{jn} g'_{kq+n} + h''_{jn} f'_{kq+n} - f_{jn} h'''_{kq+n} \\ & - g_{jn} g'''_{kq+n} - h_{jn} f'''_{kq+n} + 2(f'_{jn} g'_{kq+n} + g'_{jn} f'_{kq+n} - g_{jn} f''_{kq+n} - f_{jn} g''_{kq+n}) \\ & + 2\eta(-g''_{jn} f'_{kq+n} - f''_{jn} g'_{kq+n} + f_{jn} g'''_{kq+n} + g_{jn} f'''_{kq+n} + 4 f_{jn} f''_{kq+n} - 4 f'_{jn} f'_{kq+n}) \\ & + 4[(q+n)^2 - n^2 + 1](f_{jn} f'_{kq+n}) + 4\eta^2(f''_{jn} f'_{kq+n} - f_{jn} f'''_{kq+n})\}, \end{aligned} \tag{2.27b}$$

$$\begin{aligned} S_{3pq} = \sum_{j=q}^{p-1} \sum_{n=q+1}^{\min(j+1,\, p-j+q)} & n\{f''_{jn} h'_{kn-q} + g''_{jn} g'_{kn-q} + h''_{jn} f'_{kn-q} - f_{jn} h'''_{kn-q} \\ & - g_{jn} g'''_{kn-q} - h_{jn} f'''_{kn-q} + 2(f'_{jn} g'_{kn-q} + g'_{jn} f'_{kn-q} - g_{jn} f''_{kn-q} - f_{jn} g''_{kn-q}) \\ & + 2\eta(-g''_{jn} f'_{kn-q} - f''_{jn} g'_{kn-q} + f_{jn} g'''_{kn-q} + g_{jn} f'''_{kn-q} + 4 f_{jn} f''_{kn-q} - 4 f'_{jn} f'_{kn-q}) \\ & + 4[(n-q)^2 - n^2 + 1](f_{jn} f'_{kn-q}) + 4\eta^2(f''_{jn} f'_{kn-q} - f_{jn} f'''_{kn-q})\}. \end{aligned} \tag{2.27c}$$

The matching conditions for the third-order inner solution are

$$h_{01} \sim 2\eta^3 - \frac{4}{\pi^{\frac{1}{2}}}\eta^2 + \tfrac{1}{2}\eta, \tag{2.28}$$

$$h_{pq} \sim -2q[\gamma_{pq}\eta - (q+1)f_{pq}(\infty)\eta^2], \quad 1 \leqslant p, \tag{2.29}$$

where γ_{pq} is a constant which is defined by

$$\gamma_{pq} = \lim_{\eta\to\infty}[g_{pq}(\eta) + 2qf_{pq}(\infty)\eta]. \tag{2.30}$$

Details of this matching procedure are given in Nam (1988). The analytic solution of the first time term of the third-order approximate equation is

$$h_{01} = \operatorname{erf}\eta\,(\tfrac{8}{3}\eta^3 + \tfrac{1}{2}\eta) + \frac{e^{-\eta^2}}{\pi^{\frac{1}{2}}}(\tfrac{8}{3}\eta^2 - \tfrac{1}{12}) - \tfrac{2}{3}\eta^3 - \frac{4}{\pi^{\frac{1}{2}}}\eta^2 + \frac{1}{12\pi^{\frac{1}{2}}}, \tag{2.31}$$

which agrees with Dennis & Collins (1973*a*), but differs from Bar-Lev & Yang (1975).

Since the matching condition for the third-order solution shows that the second derivatives of the solution do not approach zero as $\eta\to\infty$, we defined $H_{pq} = e^{\frac{1}{2}\eta^2}[h''_{pq} - h''_{pq}(\infty)]$ to make H_{pq} vanish as $\eta\to\infty$.

As we go to higher approximations, the cost of numerical computation becomes large geometrically owing to the rapid increase of the right-hand sides of the equations.

3. Exponentially accelerating circular cylinder

We now suppose that the velocity of the cylinder is not a step function, but is increasing exponentially with time, according to

$$U_\infty(t) = A\,e^{ct}, \tag{3.1}$$

where A and c are constants having the dimensions of velocity and of inverse time.

We adopt $\eta = y/(\nu/c)^{\frac{1}{2}}$, and $\tau = A/(ac\,e^{ct})$. Also let

$$\Psi = 2(\nu/c)^{\frac{1}{2}}A\,e^{ct}\left[\tilde{\psi}(\eta,\theta,\tau) + \frac{(\nu/c)^{\frac{1}{2}}}{a}\tilde{\tilde{\psi}}(\eta,\theta,\tau) + \frac{(\nu/c)}{a^2}\tilde{\tilde{\tilde{\psi}}}(\eta,\theta,\tau) + O\left(\frac{(\nu/c)^{\frac{3}{2}}}{a^3}\right)\right], \tag{3.2}$$

and we follow the same procedure as that for the impulsively started case.

3.1. *First-order boundary-layer expansion*

The ordinary differential equations of the first-order boundary-layer approximation for $p+q$ odd are given as

$$f'''_{pq} - (1+p)f'_{pq} = -\delta_{0p} + (S_{1pq} + S_{2pq} - S_{3pq} - \delta_{1p}). \tag{3.3}$$

The double sums S_{ipq} are the same as given in (2.12*a*, *b*, *c*), and the boundary conditions are same as (2.13*a*, *b*).

The analytic solutions of the first few terms are easily obtainable as

$$f_{01} = e^{-\eta} + \eta - 1, \tag{3.4}$$

$$f_{12} = -1/\sqrt{2}e^{-\sqrt{2}\eta} - \eta e^{-\eta} + 1/\sqrt{2}, \tag{3.5}$$

$$f_{21} = \frac{-15+4\sqrt{2}}{2\sqrt{3}}e^{-\sqrt{3}\eta} + \sqrt{2}/2e^{-(\sqrt{2}+1)\eta} + (2\eta+\tfrac{13}{2})e^{-2\eta} + (-\eta-4+\sqrt{2})e^{-\sqrt{2}\eta} + (-\tfrac{1}{2}\eta^2+\tfrac{5}{2}\eta-4+\sqrt{2}/2)e^{-\eta} + \frac{15-4\sqrt{2}}{2\sqrt{3}} - 2\sqrt{2}+\tfrac{3}{2}, \quad (3.6)$$

$$f_{23} = (27\sqrt{3}/2-\sqrt{6})e^{-\sqrt{3}\eta} - (5\sqrt{2}/2-3)e^{-(\sqrt{2}+1)\eta} + (-2\eta-\tfrac{15}{2})e^{-2\eta} + (-\sqrt{2}\eta+\sqrt{2})e^{-\sqrt{2}\eta} + (-\tfrac{1}{2}\eta^2+\tfrac{1}{2}\eta-\sqrt{2}/2)e^{-\eta} + (-27\sqrt{3}/2+\sqrt{6}+\tfrac{9}{2}+2\sqrt{2}). \quad (3.7)$$

However it soon becomes clear that continuing to obtain analytic solutions by hand is quite impractical owing to the rapid increase of the number of terms which are generated by the combination of previous terms.

We found that the structure of the equations ensures that the solutions are exponentials multiplied by polynomials in η as in (3.7) which are generated by the combination of its predecessors. We first developed a program that finds the coefficient of each exponential function from the results of the right-hand side of (3.3). Then, since we could predict the patterns of all higher-order derivatives of the exponential function, we obtain the exact solution of each ODE by the method of undetermined coefficients. Special care should be taken whenever the particular solution obtained by this method happens to possess the same function as the homogeneous solution of that particular equation.

3.2. *Second- and third-order boundary-layer expansion*

The expressions for the ODE's of the second- and third-order boundary-layer expansion are given in Nam (1988).

The matching conditions for the second-order boundary-layer solution as $\eta \to \infty$ are

$$g_{01} \sim -\tfrac{1}{2}\eta^2 + \eta, \quad (3.8a)$$

$$g_{pq} \sim -qf_{pq}(\infty)\eta, \quad 1 \leqslant p. \quad (3.8b)$$

The analytic solutions of the first two time terms of the second-order boundary-layer equation are

$$g_{01} = e^{-\eta}\left(-\frac{\eta}{2}+\tfrac{1}{2}\right) - \frac{\eta^2}{2} + \eta - \tfrac{1}{2}, \quad (3.9)$$

$$g_{12} = e^{-\sqrt{2}\eta}\left(\frac{\eta}{2\sqrt{2}} - 13\sqrt{2}/2 - \tfrac{3}{4}\right) + e^{-\eta}(2\eta^2-\eta+12) - \sqrt{2}\eta + 13\sqrt{2}/2 - \tfrac{45}{4}. \quad (3.10)$$

More analytic solutions of second-order boundary-layer problems were computed by the computer.

We stopped using the computer for the third-order solution owing to the excessive amount of computing time required. The analytic solution of the first term of the third-order approximate equation is

$$h_{01} = e^{-\eta}(\tfrac{3}{8}\eta^2 - \tfrac{5}{8}\eta - \tfrac{1}{8}) + \tfrac{1}{2}\eta^3 - \eta^2 + \tfrac{1}{2}\eta + \tfrac{1}{8}. \quad (3.11)$$

4. Results and discussion

For the case of the impulsively started cylinder, we obtained numerical solutions of ODE's with up to 51 terms with respect to time for each of the first three orders of approximation in *Re*.

We found that our numerical solution retains from 11 to 3 significant figures at the 51st term of the first-order, and from 9 to 2 significant figures for the second-order approximate solutions. However, the third-order solution is deteriorating rapidly

compared with that of the previous two. We accept the third-order solution only up to $p = 28$ which still retains between 6 and 2 significant figures. Collins & Dennis (1973*a*) give eight, seven, and six terms of $f''_{pq}(0)$, $g''_{pq}(0)$, and $h''_{pq}(0)$, respectively. Our result and theirs are in good agreement. Concerning the small discrepancy, we believe our results are more accurate than theirs since we use an $O(h^6)$ method compared with their $O(h^4)$ method.

We found the time when the wall shear first reverses at $\theta = \pi$ as $\tau_0 = 0.321919888409$ based on the first-order solution. This agrees well with Hommel's (1983) $\tau_0 = 0.32191985$ and Cowley's (1983) $\tau_0 = 0.32191989$.

The beauty of the case of an exponentially accelerating cylinder is that we can obtain as many analytic solutions as we desire. However, because of the rapidly increasing right-hand side of the ODE's, we selected $p = 14$. For $p = 14$, f_{pq} is composed of about 1500 non-zero coefficients and g_{pq} contains about 2000 non-zero coefficients.

We checked several flow quantities in the second- and third-order solutions to investigate the nature of a singularity which appears in the classical unsteady boundary-layer solution.

4.1. *Viscous displacement velocity*

According to Cowley (1983), the so-called *viscous displacement velocity* is more sensitive to the presence of a singularity than any other of the flow quantities commonly referred to. We concentrate on the behaviour of the viscous displacement velocity of the higher-order approximate solutions around the singularity.

Since we are dealing with successive approximations, we need to define v_∞ according to each order of approximation. We define the viscous displacement velocity as

$$v_\infty = v_{1\infty} + \epsilon v_{2\infty} + \epsilon^2 v_{3\infty}, \tag{4.1}$$

where we denote the perturbation quantity $(\nu t)^{\frac{1}{2}}/a$ by ϵ and $v_{1\infty}, v_{2\infty}, v_{3\infty}$ are the first-, second-, and third-order viscous displacement velocity, respectively. We also define Ψ_1, Ψ_2, Ψ_3, $\bar{\Psi}_1$, $\bar{\Psi}_2$, and $\bar{\Psi}_3$ as the first, second, and third order of the inner- and outer-layer stream functions, respectively.

The first-order viscous displacement velocity $v_{1\infty}$ of the impulsively started cylinder flow is the radial velocity at the edge of the boundary layer of the first-order inner solution minus that of the outer solution, and we keep only the first-order term of this result as $v_{1\infty}$. Expanding the outer solution in the inner variable and collecting terms of the same order of ϵ results in

$$-\frac{1}{r}\frac{\partial}{\partial\theta}(\Psi_1 - \bar{\Psi}_1)\bigg|_{\eta\to\infty} = 4U_\infty\left[\epsilon\left(\frac{1}{\pi^{\frac{1}{2}}}\cos\theta - \sum_{p=1}^{\infty}\sum_{q=2}^{p+1}\tau^p f_{pq}(\infty)\, q\cos q\theta\right) + O(\epsilon^2)\right]. \tag{4.2}$$

Neglecting dimensional factors yields the following expression for $v_{1\infty}$:

$$v_{1\infty} = \tau^{\frac{1}{2}}\left(\frac{1}{\pi^{\frac{1}{2}}}\cos\theta - \sum_{p=1}^{\infty}\sum_{q=2}^{p+1}\tau^p f_{pq}(\infty)\, q\cos q\theta\right). \tag{4.3}$$

The expressions for the second- and third-order viscous displacement velocity are

$$v_{2\infty} = \lim_{\eta\to\infty}\tau^{\frac{1}{2}}\left\{\tfrac{1}{4}\cos\theta - \sum_{p=1}^{\infty}\sum_{q=2}^{p+1}\tau^p[g_{pq}(\eta) + 2q\eta f_{pq}(\infty)]\, q\cos q\theta\right\}, \tag{4.4}$$

$$v_{3\infty} = \lim_{\eta\to\infty}\tau^{\frac{1}{2}}\left\{-\frac{1}{12\pi^{\frac{1}{2}}}\cos\theta - \sum_{p=1}^{\infty}\sum_{q=2}^{p+1}\tau^p[h_{pq}(\eta) + 2qg_{pq}(\eta)\,\eta + 2q(q-1)\,\eta^2 f_{pq}(\infty)]\, q\cos q\theta\right\}. \tag{4.5}$$

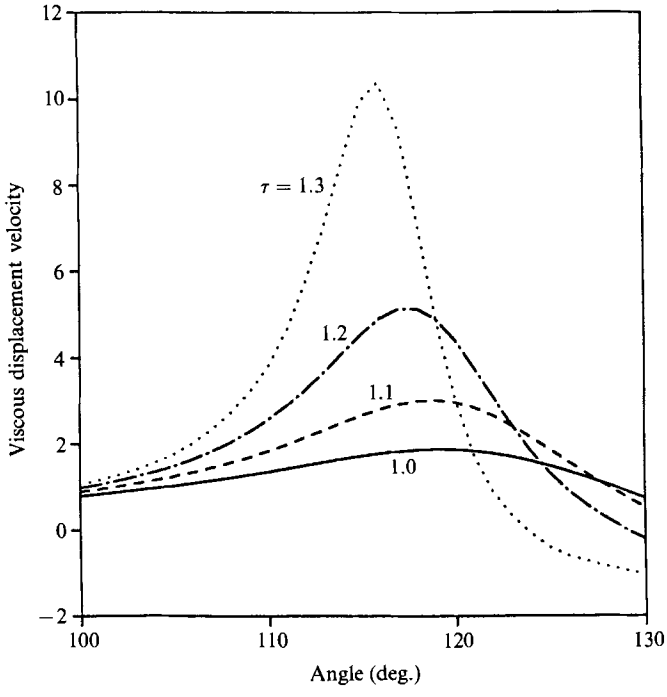

FIGURE 2. The first-order viscous displacement velocity for the impulsively started cylinder: it is smooth at an early stage and rapidly increasing as τ increases. The maximum, which is believed to be a symptom of singularity, moves to the left. The graph was drawn from a [24/25] Padé approximant.

Note that the $O(\epsilon)$ term vanished in the expression for $v_{2\infty}$, and the $O(\epsilon)$ and $O(\epsilon^2)$ terms disappeared in that for $v_{3\infty}$ owing to the second- and third-order approximation, respectively.

By an analogous procedure, we also find $v_{1\infty}$ and $v_{2\infty}$ for the exponentially accelerating cylinder as

$$v_{1\infty} = \tau^{\frac{1}{2}}\left(\cos\theta - \sum_{p=1}^{\infty}\sum_{q=2}^{p+1}\tau^p f_{pq}(\infty)\, q\cos q\theta\right), \tag{4.6}$$

$$v_{2\infty} = \lim_{\eta\to\infty}\tau^{\frac{1}{2}}\left[\tfrac{1}{2}\cos\theta - \sum_{p=1}^{\infty}\sum_{q=2}^{p+1}\tau^p(g_{pq}(\eta)+2q\eta f_{pq}(\infty))\, q\cos q\theta\right], \tag{4.7}$$

where we denote $(\nu/c)^{\frac{1}{2}}$ by ϵ. We have used the [24/25] Padé approximant to draw graphs for the first- and second-order solutions of the impulsively started cylinder, and the [13/14] Padé approximant for the third-order solution. Without using Padé approximants, we could not draw meaningful graphs as time is increasing.

The singularity that appears in the viscous displacement velocity of the first-order solution agrees well with that of van Dommelen & Shen (1980), Cowley (1983), and Ingham (1984). They show that the singularity of the classical boundary-layer solution is located near $\theta \approx 111°$ at $\tau \approx 1.5$.

Figure 2 shows that the first-order viscous displacement velocity grows rapidly as τ approaches 1.5. The locations of the maxima suggest a singularity at less than $\theta = 115°$. The Padé approximants reveal the location of the singularity between 110° and 112°. We take the singularity to be located at $\theta \approx 111°$ as van Dommelen & Shen (1980), Cowley (1983), and Ingham (1984) claim. The Padé approximants from

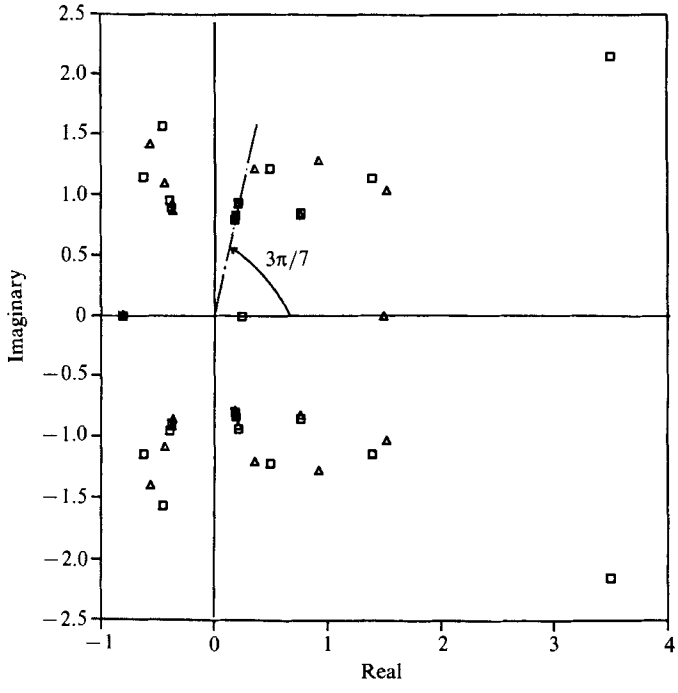

FIGURE 3. The zeros (□) and poles (△) in the complex domain of the [24/25] Padé approximant to the first-order viscous displacement velocity for the impulsively started cylinder: the nearest singularity on the real axis is 1.494 when θ is fixed as 111°.

[19/20] to [24/25] with the fixed angle at 111° show that the real poles gather around 1.494. This indicates that the location of the nearest singularity on the real axis at $\theta = 111°$ is $\tau \approx 1.494$. Figure 3 shows poles and zeros of the [24/25] Padé approximant in the complex domain.

Figure 4 shows that the second-order viscous displacement velocity has a similar singular behaviour to that of the first-order solution but with opposite sign and bigger magnitude. The Padé approximants for the second-order solution show that the location of the singularity is near $\theta = 111°$ with even less error range than that of the first one. The Padé approximants from [19/20] to [24/25] of the second-order solution indicate that the location of the nearest singularity on the real axis at $\theta = 111°$ is $\tau \approx 1.39$.

For the third-order solution, we do not have enough terms to give a reliable quantitative result and so figure 5 is only qualitative. However, it suggests that the behaviour of the third-order viscous displacement velocity is opposite to that of the second-order but with bigger magnitude.

Another interesting point that we can draw from these three viscous displacement velocity components is that at each order the series for the viscous displacement velocity has the same repeated sign pattern of period 14. For a fixed angle, say $\theta = 111°$, we have done a series solution of 51 terms for the first- and second-, and 29 terms for the third-order approximation with respect to time. The coefficients of the first-order solution develop a sign pattern of $- - + + - - - + + - - + + +$ beginning with the fourteenth term. The second-order solution shows the same pattern starting from the sixteenth term. The third-order solution shows the same pattern starting from the fourteenth term. According to Li (1982), this sign pattern

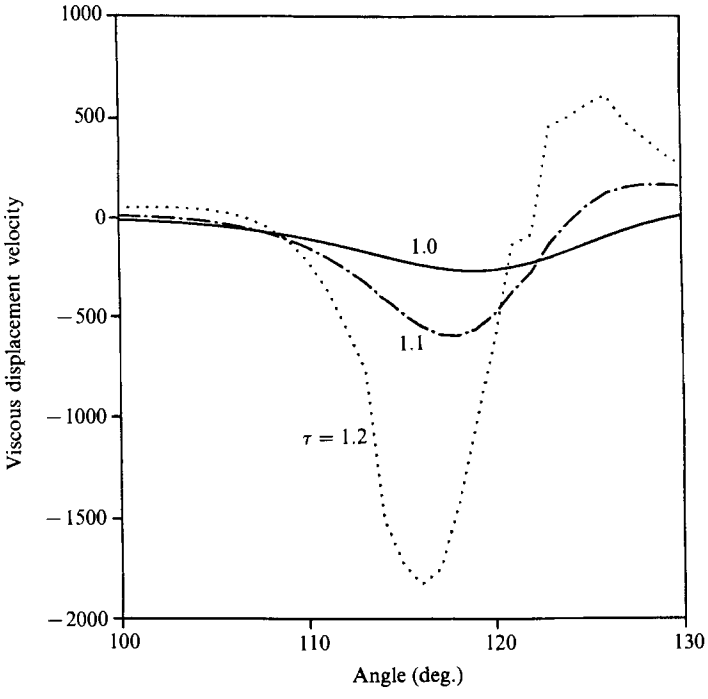

FIGURE 4. The second-order displacement velocity for the impulsively started cylinder: this suggests that the singularity is located left of $\theta \approx 115°$ as τ approaches 1.5.

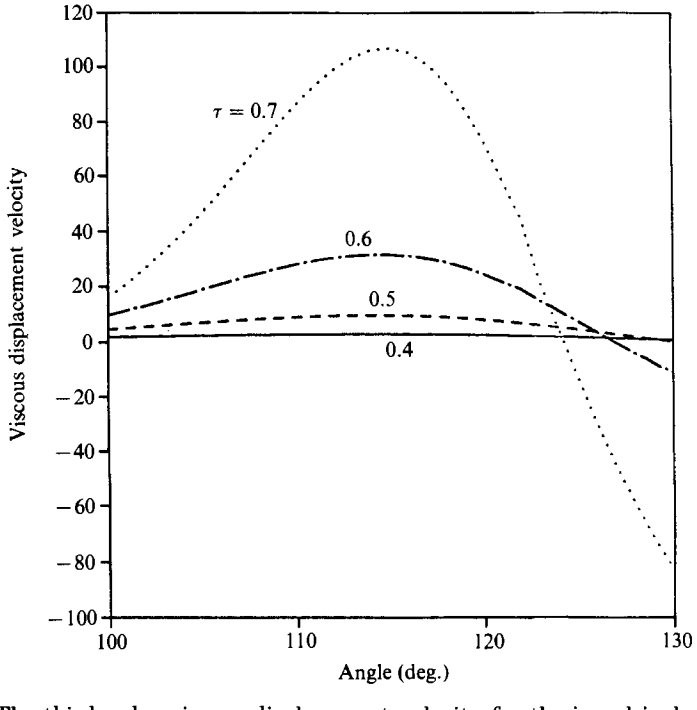

FIGURE 5. The third-order viscous displacement velocity for the impulsively started cylinder: it grows fast as time progresses. The magnitude is much greater than that of the second-order solution but with opposite sign.

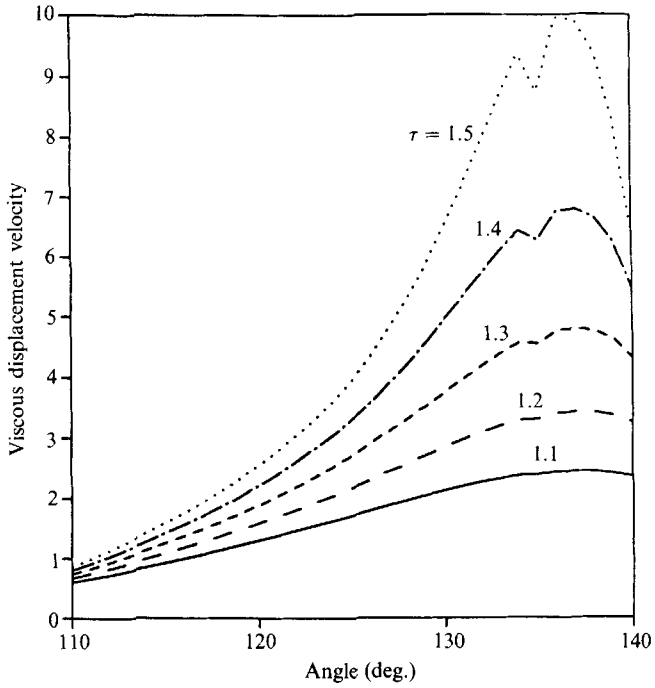

FIGURE 6. The first-order viscous displacement velocity for the exponentially accelerating cylinder: it starts to show a breakdown of the smooth curve and rapid increase of magnitude around $\theta \approx 138°$ as time progresses. This suggests the possibility of a singularity which may be located at the left of $\theta \approx 138°$ and at $\tau > 1.5$.

indicates that the nearest singularities are a conjugate pair located at angles $\pm 3\pi/7$ from the positive axis in the complex plane. The Padé approximants from [19/20] to [24/25] of the first-order viscous displacement velocity show that the nearest singularities lie at about 0.188 ± 0.790i, which corresponds to angles of $\pm 2.98\pi/7$. Figure 3 shows that this is the angle to the nearest pole. This result agrees quite well with the expected value $\pm 3\pi/7$. The nearest singularity from the second-order viscous displacement velocity coincides even better with the expected value. It is about 0.181 ± 0.790i, which corresponds to angles of $\pm 3.00\pi/7$ in the complex plane. While this agreement between sign patterns and nearest singular points is reassuring, it cannot be of much help in improving a series solution unless the nearest singular point is located on the real axis.

We have obtained 15 terms of the expansion in powers of time up to the second-order approximation for the exponentially accelerative cylinder. This number of terms is probably not sufficient to quantify any result with confidence. However, it seems to be adequate to give the character of the viscous displacement velocity in a qualitative sense.

Though this flow does not involve singular movements either at the initial stage or thereafter, the behaviour of its viscous displacement velocity is very similar to that of impulsive movement which is inherently singular at the initial stage.

Figure 6 shows that the maximum viscous displacement velocity, which may be a symptom of a singularity, builds up around $\theta \approx 137°$, and the maximum moves to the left as time progresses, as for the impulsively started cylinder. The second-order viscous displacement velocity in figure 7 also shows the same pattern of growing

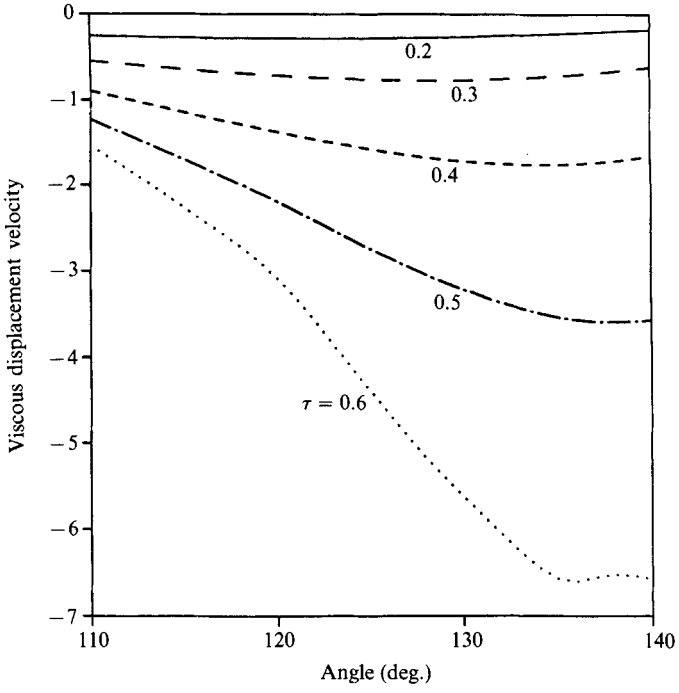

FIGURE 7. The second-order viscous displacement velocity for the exponentially accelerating cylinder: it shows a growing magnitude with opposite sign compared with the first-order viscous displacement velocity. It also shows that the second-order viscous displacement velocity grows rapidly at the same place as the first-order one.

magnitude with opposite sign to that of the first-order viscous displacement velocity, as it did in the case of the impulsively started cylinder.

4.2. *Skin friction S_f along the wall of the cylinder*

Though there is as yet no clear consensus on a definition of unsteady separation, and the skin friction is not as sensitive an indicator of any singularity as either viscous displacement velocity or viscous displacement thickness, skin-friction data should be included for the sake of completeness. The shear force along a surface is computed by

$$S_f = \mu \left.\frac{\partial u}{\partial y}\right|_{y=0}. \tag{4.8}$$

Expressing u in terms of the stream function of the impulsively started cylinder flow yields

$$S_f = \rho U_\infty \left(\frac{\nu U_\infty}{a}\right)^{\frac{1}{2}} \left\{ \sum_{p=0}^{\infty} \tau^{p-\frac{1}{2}} \sum_{q=1}^{p+1} [f''_{pq}(0) + \epsilon g''_{pq}(0) + \epsilon^2 h''_{pq}(0) + \ldots] \sin q\theta \right\}. \tag{4.9}$$

We define the non-dimensional shear force at each order of approximation as

$$S_{f1} = \sum_{p=0}^{\infty} \tau^{p-\frac{1}{2}} \sum_{q=1}^{p+1} f''_{pq}(0) \sin q\theta, \tag{4.10}$$

$$S_{f2} = \sum_{p=0}^{\infty} \tau^{p-\frac{1}{2}} \sum_{q=1}^{p+1} g''_{pq}(0) \sin q\theta, \tag{4.11}$$

$$S_{f3} = \sum_{p=0}^{\infty} \tau^{p-\frac{1}{2}} \sum_{q=1}^{p+1} h''_{pq}(0) \sin q\theta, \tag{4.12}$$

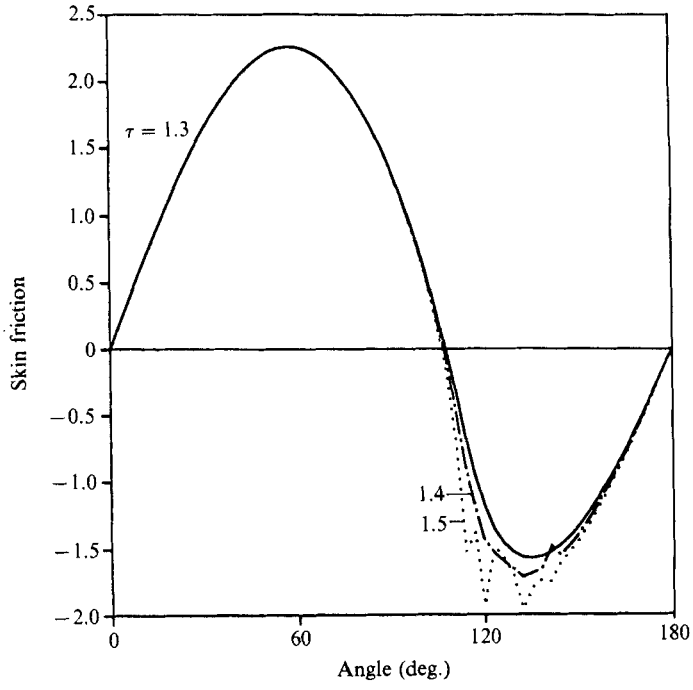

FIGURE 8. The first-order skin friction for the impulsively started cylinder: a breakdown of the smooth curve starts to appear at $\tau \approx 1.4$ around $\theta \approx 120°$.

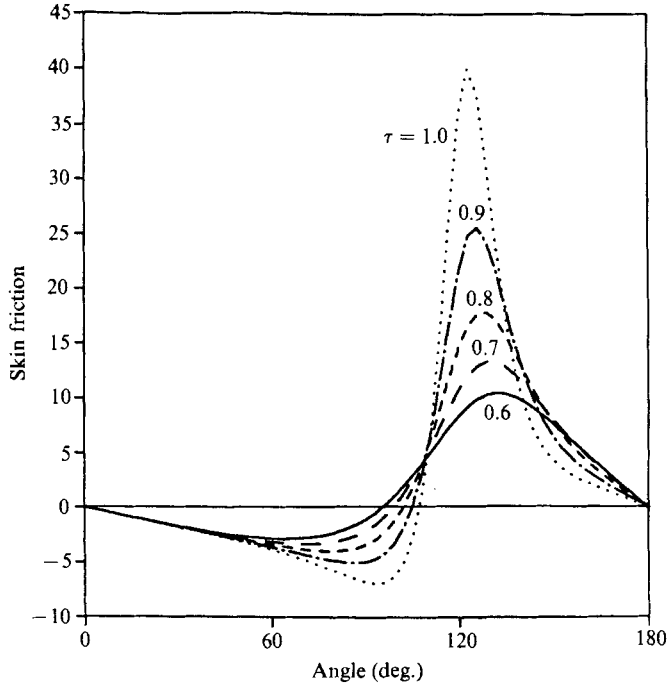

FIGURE 9. The second-order skin friction for the impulsively started cylinder: rapidly increasing second-order skin friction shows that the maximum moves to the left of $\theta \approx 120$ as time increases.

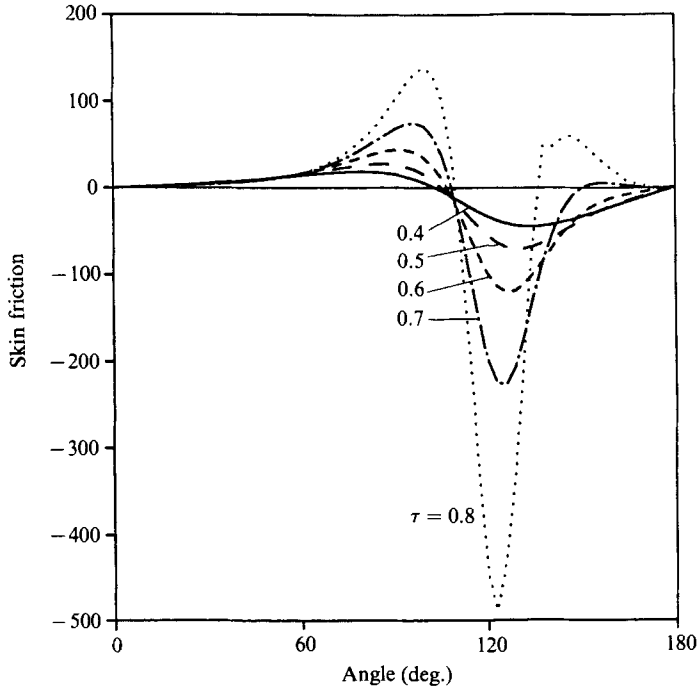

FIGURE 10. The third-order skin friction for the impulsively started cylinder: it rapidly increases as time increases. The minimum moves to the left of $\theta \approx 120$ and magnitude grows fast with an opposite sign.

where the subscript 1, 2, 3 corresponds to each order of approximation. The same definitions are used for the exponentially accelerating cylinder.

We have used [24/25] Padé approximants to plot S_{f1}, and S_{f2}, and used a [13/14] approximant for S_{f3} for the impulsively started cylinder.

The graph of S_{f1} indicates some abnormality as $\tau \geqslant 1.4$, see figure 8. S_{f2}, which is shown in figure 9, confirms the tendency that we observed for the viscous displacement velocity. The singularity seems to develop in the same place but with bigger amplitude and with an opposite sign. S_{f3} in figure 10 also seems to lead to the same conclusion. We do not have enough terms to draw any meaningful plot beyond $\tau = 0.8$, but the point of singularity seems to move left of $\theta \approx 120°$ as time increases.

For the exponentially accelerating cylinder S_{f2} has an opposite sign and bigger magnitude than S_{f1}.

4.3. *Pressure distribution along the wall*

In the classical boundary-layer approximation, the pressure distribution is given by the first-order potential-flow pressure distribution, which leads to the Goldstein singularity in the steady-flow solution. Our solution, which uses successive approximations, has corrections for the pressure according to each order of approximation. The pressure distribution in the higher-order solutions will show adjustments to the effects of viscosity, vorticity, etc. calculated by the lower-order solutions.

We non-dimensionalize the pressure with $1/2\rho U_\infty^2$. We expand dimensionless p as

$$p = p_1 + \epsilon p_2 + \epsilon^2 p_3 + \ldots. \tag{4.13}$$

Since the third-order solution does not have a sufficient number of terms, we check only p_1 and p_2 terms.

After transforming the cylindrical coordinates to boundary-layer stretched coordinates, the Navier–Stokes equation gives

$$\frac{\partial p}{\partial \theta} = 4\tilde{\psi}_{\tau\tau} + \frac{2}{\tau}\eta\tilde{\psi}_{\eta\eta} + 8\tilde{\psi}_{\theta}\tilde{\psi}_{\eta\eta} - 8\tilde{\psi}_{\eta}\tilde{\psi}_{\eta\theta} + \frac{1}{\tau}\tilde{\psi}_{\eta\eta\eta}$$

$$+\epsilon\Big(-8\eta\tilde{\psi}_{\eta\tau} + \frac{4}{\tau}\eta^2\tilde{\psi}_{\eta\eta} - 4\tilde{\tilde{\psi}}_{\tau\tau} - \frac{2}{\tau}\tilde{\tilde{\psi}}_{\eta} + \frac{2}{\tau}\eta\tilde{\tilde{\psi}}_{\eta\eta} + 8\tilde{\tilde{\psi}}_{\theta}\tilde{\psi}_{\eta\eta} + 8\tilde{\psi}_{\theta}\,\tilde{\tilde{\psi}}_{\eta\eta}$$

$$-8\tilde{\psi}_{\eta}\tilde{\tilde{\psi}}_{\eta\theta} - 8\tilde{\tilde{\psi}}_{\eta}\tilde{\psi}_{\eta\theta} + 16\tilde{\psi}_{\eta}\tilde{\psi}_{\theta} + \frac{2}{\tau}\eta\tilde{\psi}_{\eta\eta\eta} + \frac{1}{\tau}\tilde{\tilde{\psi}}_{\eta\eta\eta} + \frac{2}{\tau}\tilde{\psi}_{\eta\eta}\Big) + O(\epsilon^2), \tag{4.14}$$

$$\frac{\partial p}{\partial \eta} = \epsilon(16\tilde{\psi}_{\eta}^2) + O(\epsilon^2). \tag{4.15}$$

Equation (4.15) shows that the pressure gradient in the r-direction is zero for the first-order solution, which is the classical boundary-layer assumption. However it is no longer zero for the higher-order solutions.

The derivatives of the pressure distribution along the surface from (4.14) are

$$\left.\frac{\partial p_1}{\partial \theta}\right|_{\eta=0} = -4\sin 2\theta, \tag{4.16}$$

and

$$\left.\frac{\partial p_2}{\partial \theta}\right|_{\eta=0} = \sum_{p=0}^{\infty}\sum_{q=1}^{p+1} \tau^{p-1}[2f''_{pq}(0) + g'''_{pq}(0)]\sin q\theta. \tag{4.17}$$

Though the stagnation pressure is a function of both time and Re, we set the dimensionless pressure at the stagnation point be 1 as a reference point to compare with the pressure along the surface. We obtain the first-order pressure distribution along the surface as

$$p_1 = 2\cos 2\theta - 1, \tag{4.18}$$

which is simply the first-order potential-flow pressure distribution.

Through the inner- and outer-layer matching process, the second-order outer-layer contains $O(\epsilon)$ correction terms which are the result of the viscous effect in the first-order boundary-layer solution. The first correction in the pressure distribution along the surface is given from (4.17) as

$$p_2 = \sum_{p=0}^{\infty}\sum_{q=1}^{p+1} -\tau^{p-1}[2f''_{pq}(0) + g'''_{pq}(0)]\frac{1}{q}\cos q\theta + \text{constant}, \tag{4.19}$$

where the constant ensures that p_2 becomes zero at the front stagnation point. Figure 11 shows the second-order pressure distribution at different times. The pressure along the surface also shows the same behaviour as we have seen for the viscous displacement velocity and skin friction. The rapidly increasing pressure around the singularity reveals that the boundary-layer assumptions break down around there.

4.4. *Conclusion*

Two flows have been considered: one past an impulsively started cylinder and the other past an exponentially accelerating cylinder.

Though the appearance of the singularity in the exponentially accelerating flow was suppressed a little longer than that of the impulsively started flow, owing to slow

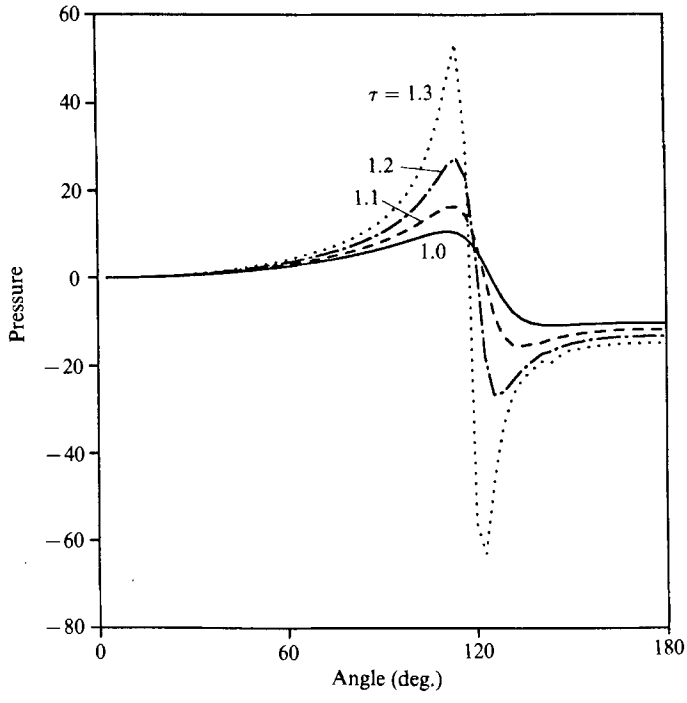

FIGURE 11. The second-order pressure distribution along the surface: rapidly increasing pressure as $\tau \geqslant 1.3$ reveals that the singularity is imminent and the boundary-layer assumptions certainly break down around that point.

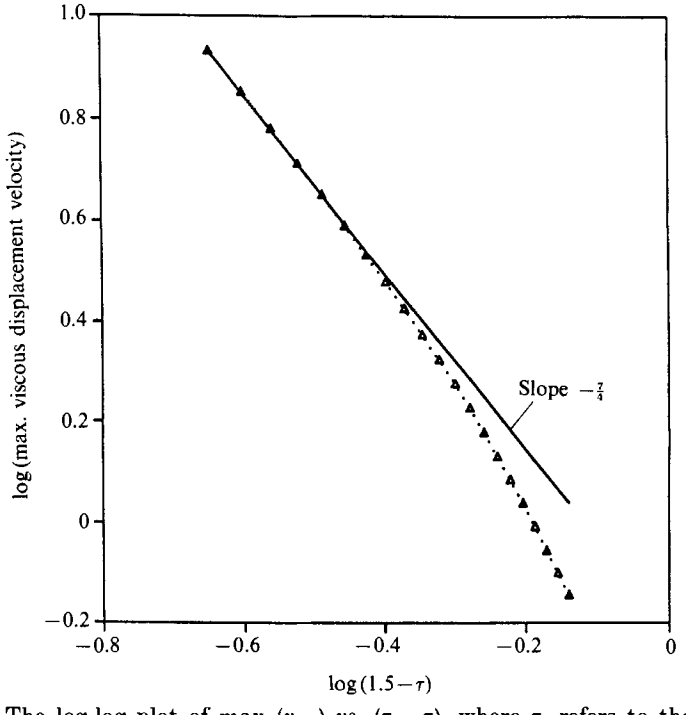

FIGURE 12. The log-log plot of max $(v_{1\infty})$ *vs.* $(\tau_s - \tau)$, where τ_s refers to the time at which the singularity take place taken as 1.5. The slope near the singularity seems to be $-\frac{7}{4}$, and $0.8 \leqslant \tau \leqslant 1.3$.

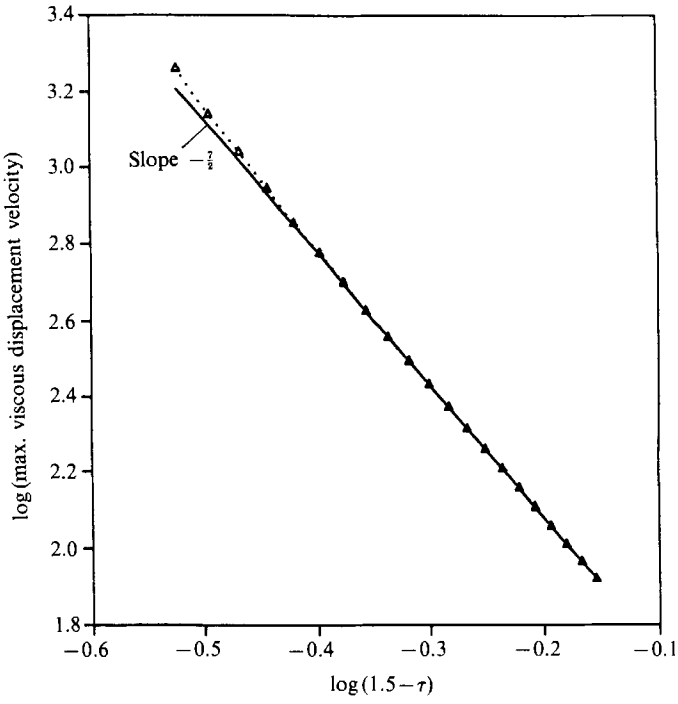

FIGURE 13. The log-log plot of max $(v_{2\infty})$ *vs.* $(\tau_s-\tau)$. The slope near the singularity seems to be $-\frac{7}{2}$, and $0.8 \leqslant \tau \leqslant 1.2$.

start of the flow, the behaviour of the viscous displacement velocities in both flows is very similar. This similarity excludes the possibility of the singularity being induced by the impulsive movement, which is singular by its nature.

The evidence from viscous displacement velocity, skin friction, and pressure distribution that we have gathered shows that the singularity effect is compounded in higher approximations. Figure 12 shows that the maximum $v_{1\infty}$ grows like $(\tau_s-\tau)^{-\frac{7}{4}}$ near the singularity, where τ_s refers to the dimensionless time at which the singularity takes place. The result confirms that of Cowley (1983) and Ingham (1984). Figure 13 shows that the maximum $v_{2\infty}$ grows like $(\tau_s-\tau)^{-\frac{7}{2}}$ from a quite early time to near the singularity. This reveals that $v_{2\infty}$ grows like

$$v_{2\infty} \sim -v_{1\infty}^2, \tag{4.20}$$

around the singularity. Figure 14 suggests that the maximum of $v_{3\infty}$ might grow like $(\tau_s-\tau)^{-\frac{37}{4}}$. However, this is inconclusive owing to the lack of sufficient terms to deduce a reliable result.

The apparent location of the nearest singularity on the real axis for the second-order impulsively started cylinder solution is a little different from that of the first-order one: 1.39 *vs.* 1.494. However the nearest singularities on the real axis from [19/20] to [24/25] Padé approximants for the second-order solution show that the radius of convergence is increasing as the degree of approximant increases. This confirms our belief that if we could use more coefficients in the Padé approximants, exactly the same value of τ would result for both cases.

The analysis shows that the singularities in the higher-order approximation have alternating signs and increasing magnitudes, thereby attempting to remove the effects of the singularity of the lower-order approximate solution. However this

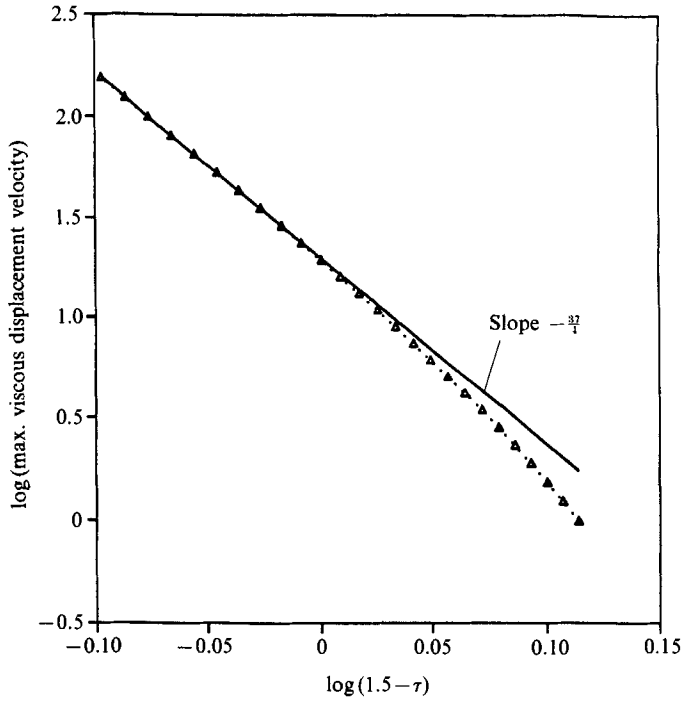

FIGURE 14. The log-log plot of max $(v_{3\infty})$ *vs.* $(\tau_s - \tau)$: The slope near the singularity seems to be $-\frac{37}{4}$, and $0.2 \leqslant \tau \leqslant 0.7$. Since we do not have enough terms of the solution to predict the behaviour of $v_{3\infty}$ near the singularity with reasonable accuracy, this value is inconclusive.

desperate attempt at removing a singularity by superposing even stronger singularities with alternating signs makes the solution worse around the singular point.

Since the Navier–Stokes equations should not yield any singularity, it is obvious that it has been introduced by transforming (2.1) into (2.3) based on the thin-boundary-layer assumption. Therefore the compounding singularity in the higher-order solutions reveals the limitation of the boundary-layer approximation. In this sense, the appearance of a singularity could be a strong indication of the imminent separation.

REFERENCES

BAR-LEV, M. & YANG, H. T. 1975 Initial flow field over an impulsively started circular cylinder. *J. Fluid Mech.* **72**, 625–647.

BLASIUS, H. 1908 Grenzschichten in Flüssigkeiten mit kleiner Reibung. *Z. Math. Phys.* **56**, 1–37.

CEBEI, T. 1979 The laminar boundary-layer on a circular started impulsively from rest. *J. Comput. Phys.* **31**, 153–172.

COLLINS, W. M. & DENNIS, S. C. R. 1973*a* The initial flow past an impulsively started circular cylinder. *Q. J. Mech. Appl. Maths* **26**, 53–75.

COLLINS, W. M. & DENNIS, S. C. R. 1973*b* Flow past an impulsively started circular cylinder. *J. Fluid Mech.* **60**, 105–127.

COWLEY, S. J. 1983 Computer extension and analytic continuation of Blasius' expansion for impulsive flow past a circular cylinder. *J. Fluid Mech.* **135**, 389–405.

FOX, L. 1957 *The Numerical Solution of Two-Point Boundary Problem in Ordinary Differential Equations.* Oxford University Press.

GOLDSTEIN, S. 1948 On laminar boundary-layer flow near a point of separation. *Q. J. Mech. Appl. Maths* **1**, 43–69.

GOLDSTEIN, S. & ROSENHEAD, L. N. 1936 Boundary layer growth. *Proc. Camb. Phil. Soc.* **32**, 392–401.

HENKES, R. A. & VELDMAN, A. E. P. 1987 On the breakdown of the steady and unsteady interacting boundary-layer description. *J. Fluid Mech.* **179**, 513–529.

HOMMEL, M. J. 1983 The laminar unsteady flow of a viscous fluid away from a plane stagnation. *J. Fluid Mech.* **132**, 407–416.

INGHAM, D. B. 1984 Unsteady separation. *J. Comput. Phys.* **53**, 90–99.

LI, JIACHUN 1982 Singularity criteria for perturbation series. *Scientia Sinica* A, vol. **25**, 593.

NAM, S. 1988 Higher order boundary-layer solution for unsteady motion of a circular cylinder. Ph.D. thesis, Stanford University, Stanford, CA.

SEARS, W. R. & TELIONIS, D. P. 1971 Unsteady boundary-layer separation. In *Recent Research on Unsteady Boundary Layers* (ed. E. A. Eichelbrenner), p. 404. Quebec: Laval University Press.

TELIONIS, D. P. & TSAHALIS, D. TH. 1974 Unsteady laminar separation over impulsively moved cylinders. *Acta Astronautica* **1**, 1484–1505.

VAN DOMMELEN, L. L. & SHEN, S. F. 1980 The spontaneous generation of singularity in a separation laminar boundary layer, *J. Comput. Phys.* **38**, 125–140.

VAN DYKE, M. 1975 *Perturbation Method in Fluid Mechanics.* Stanford: Parabolic.

WANG, C. Y. 1967 The flow past a circular cylinder which is started impulsively from rest. *J. Math. Phys.* **46**, 195–202.

WANG, K. C. 1979 Unsteady boundary layer separation. *MML Tr* 79-16c, Martin Marietta Lab., Baltimore.

WATSON, E. J. 1955 Boundary-layer growth. *Proc. R. Soc. Lond.* A **231**, 104–116.